Department of Applied Mechanics

Sea ice ridge keel punch through experiments: model experiments and numerical modeling with discrete and combined finite-discrete element methods

Arttu Polojärvi

Aalto University

DOCTORAL DISSERTATIONS

Aalto University publication series
DOCTORAL DISSERTATIONS 50/2013

Sea ice ridge keel punch through experiments: model experiments and numerical modeling with discrete and combined finite-discrete element methods

Arttu Polojärvi

A doctoral dissertation completed for the degree of Doctor of Science (Technology) to be defended, with the permission of the Aalto University School of Engineering, at a public examination held at the lecture hall K1/216 of the school on the 12th of April, 2013, at 12 noon.

Aalto University
School of engineering
Department of applied mechanics
Mechanics of Materials

Supervising professor
Jukka Tuhkuri

Thesis advisor
Jukka Tuhkuri

Preliminary examiners
Professor Knut Høyland
Norwegian University of Science and Technology
Norway

Professor YT Feng
Swansea University
United Kingdom

Opponents
Professor Knut Høyland
Norwegian University of Science and Technology
Norway

Professor Frédéric Victor Donzé
Joseph Fourier University
France

Aalto University publication series
DOCTORAL DISSERTATIONS 50/2013

ISBN 978-952-60-5081-2 (printed)
ISBN 978-952-60-5082-9 (pdf)
ISSN-L 1799-4934
ISSN 1799-4934 (printed)
ISSN 1799-4942 (pdf)
http://urn.fi/URN:ISBN:978-952-60-5082-9

Unigrafia Oy
Helsinki 2013

Finland

441 697
Printed matter

Aalto University

Abstract

Aalto University, P.O. Box 11000, FI-00076 Aalto www.aalto.fi

Author
Arttu Polojärvi

Name of the doctoral dissertation
Sea ice ridge keel punch through experiments: model experiments and numerical modeling with discrete and combined finite-discrete element methods

Publisher School of Engineering

Unit Department of applied mechanics

Series Aalto University publication series DOCTORAL DISSERTATIONS 50/2013

Field of research Mechanics of Materials

Manuscript submitted 15 October 2012 **Date of the defence** 12 April 2013

Permission to publish granted (date) 17 December 2012 **Language** English

☐ **Monograph** ☒ **Article dissertation (summary + original articles)**

Abstract

Simulations and laboratory-scale experiments were performed to study sea ice ridge keel punch through experiments and ice rubble behavior in them. The punch through experiments are an important method for deriving ice rubble properties, yet the interpretation of the experiment results is far from straightforward. Anyhow, accurate interpretation is important for the material modeling of ice rubble, and further for an accurate modeling of the ice rubble related problems needed when designing marine structures in ice covered waters.

The experimental work was performed using rubble consisting of plastic blocks. Plastic blocks made it possible to study of experimental method itself, because the interpretation of the experiment results was simplified from that of the experiments with ice rubble. The effect of indentor velocity was experimentally studied, as earlier laboratory-scale punch through experiments have suggested that the ice rubble sheer strength depends on the loading rate. The loading rate dependency of the rubble shear strength was found to be likely related to the experimental set-up rather than to the rubble material.

Simulations of punch through experiments were performed using a three dimensional discrete element method and a two dimensional combined finite discrete element method. In both of these methods, rubble is modelled as a discontinuum. The methods were developed during this work for the research on ice mechanics. Simulations of punch through experiments on non-cohesive rubble were performed using the three dimensional discrete numerical model. A technique for modeling freeze bonds was developed within the framework of two dimensional combined finite discrete element method simulations.

The simulations helped to provide insight on the analysis of the punch through experiment results. The simulation results clearly showed that the evolution of the deformation patterns was related to the load records in the experiments. In the case of partly consolidated rubble, the initial failure patterns of the rubble were observed to be related to the measured maximum force values. Furthermore, the behavior that has been earlier understood to be the result of rubble material softening was in fact shown to be due to changes in the rubble geometry during the experiment. The discontinuous modeling of rubble showed that physical phenomena could potentially be rendered out from the more traditional continuum models. These phenomena included, for example, the importance of tensile freeze failures in the failure process of partly consolidated rubble.

Keywords Ice mechanics, punch through tests, ice loads, arctic offshore structures, discrete element method, combined finite-discrete element method, discontinuous materials, numerical modeling

ISBN (printed) 978-952-60-5081-2 **ISBN (pdf)** 978-952-60-5082-9

ISSN-L 1799-4934 **ISSN (printed)** 1799-4934 **ISSN (pdf)** 1799-4942

Location of publisher Espoo **Location of printing** Helsinki **Year** 2013

Pages 123 **urn** http://urn.fi/URN:ISBN:978-952-60-5082-9

Aalto-yliopisto

Tiivistelmä

Aalto-yliopisto, PL 11000, 00076 Aalto www.aalto.fi

Tekijä
Arttu Polojärvi

Väitöskirjan nimi
Ahtojäävallin kölin lujuus: mallikokeita ja simulointeja diskreetti- sekä yhdistetyllä diskreetti- ja elementtimenetelmällä

Julkaisija Insinööritieteiden korkeakoulu

Yksikkö Sovelletun mekaniikan laitos

Sarja Aalto University publication series DOCTORAL DISSERTATIONS 50/2013

Tutkimusala Lujuusoppi

Käsikirjoituksen pvm 15.10.2012 **Väitöspäivä** 12.04.2013

Julkaisuluvan myöntämispäivä 17.12.2012 **Kieli** Englanti

☐ **Monografia** ☒ **Yhdistelmäväitöskirja (yhteenveto-osa + erillisartikkelit)**

Tiivistelmä

Ahtojäävallin kölin materiaaliominaisuuksia mitataan tavallisimmin kokeilla, joissa levymäinen työntyri painetaan vallimassaan samalla kun työntyriin kohdistuva voima mitataan. Vaikka koemenetelmä on tärkeä ja paljon käytetty, kokeiden tulosten tulkitseminen on hyvin vaikeaa. Toisaalta tulosten tarkka tulkitseminen on välttämätöntä kölin materiaalin tarkassa mallinnuksessa, jota puolestaan tarvitaan Arktisten merirakenteiden suunnittelussa. Tässä työssä kyseisiä kokeita on tutkittu sekä simuloimalla että kokeellisesti.

Työn kokeellisessa osassa tehtiin laboratoriossa kokeita kölimassalla, joka koostui muovikappaleista jääkappaleiden sijaan. Tavoitteena kokeissa oli tutkia itse koejärjestelyä ja sen vaikutuksia tuloksiin ja muovikappaleita käytettiin tuloksiin vaikuttavien ilmiöiden lukumäärän vähentämiseksi. Erityisesti tarkasteltiin kuormitusnopeuden vaikutusta, koska aikaisempien laboratoriokokeiden perusteella on epäilty vallin leikkauslujuuden kasvavan kuormitusnopeuden kasvaessa. Tässä työssä näytettin, että tämä leikkauslujuuden kasvuksi tulkittu ilmiö johtuu todennäköisesti koejärjestelystä vallin materiaalin sijaan.

Työssä kokeita mallinnettin käyttäen sekä kolmiulotteista diskreettielementtimenetelmää, että kaksiulotteista yhdistettyä elementti- ja diskreettielementtimenetelmää. Molemmissa mallinnustekniikoissa valli mallinnetaan epäjatkuvana materiaalina. Tekniikoita kehitettiin työn aikana erityisesti jäämekaniikan ongelmiin sopiviksi. Vallia, jossa jääkappaleet eivät olleet yhteenjäätyneet, mallinnettiin kolmiulotteisella diskreettielementtimenetelmällä, kun taas osittain jäätyneen vallin mallinnuksessa käytettiin kaksiulotteista yhdistettyä elementti- ja diskreettielementtimenetelmää. Jälkimmäisen mallinnustekniikan yhteyteen kehitettiin menetelmä jääkappaleita yhteensitovien sidosten mallintamiseksi.

Simulaatioiden avulla voitiin tarkastella ja analysoida kokeita yksityiskohtaisesti. Mallinnuksen perusteella löydettiin selkeä yhteys vallin deformaatiokentän kehittymisen ja mitattujen kuormien välille. Toisaalta osittain jäätyneen vallin tapauksessa löydettiin yhteys maksimikuorman ja vallin ensimmäisen vaurion geometrian välille. Lisäksi mallin perusteella voitiin näyttää, että aikaisemmin vallin materiaalin pehmenemiseksi tulkittu ilmiö selittyykin vallin deformaatiokentän ja vallin geometrian muutoksilla kokeen aikana. Käyteyt epäjatkuvat mallinnusmenetelmät paljastivat ilmiöitä, joita ei esiinny vallimassan kontinuumimallinnuksessa. Esimerkkinä näistä ilmiöistä voidaan mainita kappaleiden välisten sidosten vedosta johtuvien vaurioiden suhteellisen suuri merkitys.

Avainsanat jäämekaniikka, ahtojäävallin lujuus, jääkuormat, arktiset merirakenteet, diskreettielementtimenetelmä, yhdistetty diskreetti- ja elementtimenetelmä, epäjatkuvat materiaalit, numeerinen mallinnus

ISBN (painettu) 978-952-60-5081-2 **ISBN (pdf)** 978-952-60-5082-9

ISSN-L 1799-4934 **ISSN (painettu)** 1799-4934 **ISSN (pdf)** 1799-4942

Julkaisupaikka Espoo **Painopaikka** Helsinki **Vuosi** 2013

Sivumäärä 123 **urn** http://urn.fi/URN:ISBN:978-952-60-5082-9

Preface

During the research leading to this thesis, my work has been funded by the Ministry of Education of Finland through the National Graduate School in Engineering Mechanics, Academy of Finland, Graduate Program of the Aalto University School of Engineering, Tekes – the Finnish Funding Agency for Technology and Innovation, and the Aalto University Department of Applied Mechanics. This financial support is gratefully acknowledged.

I am grateful to my supervisor Jukka Tuhkuri for letting me work on this interesting subject. His ideas, comments and suggestions during this work have been very valuable. He has also helped by providing good working conditions at the research group on Solid Mechanics.

I am also very thankful to my good friend Jani Paavilainen, who I have worked with at the research group on Solid Mechanics. Discussions with him on this work, on science, and on countless other issues have been a lot of help during these years.

I would also like to thank my parents, brother and all of my friends who have all helped me more than they know. Finally, I would like to thank my dear girlfriend Anna Estarriola who has had to go through quite a bit of stuff because of this work. I really do appreciate your patience and unlimited support.

Helsinki, January 4, 2013,

Arttu Polojärvi

Contents

List of Publications

This thesis consists of an overview and of the following publications which are referred to in the text by their Roman numerals.

I Arttu Polojärvi and Jukka Tuhkuri. 3D discrete numerical modeling of ridge keel punch through tests. *Cold Regions Science and Technology*, 56, 18-29, 2009.

II Arttu Polojärvi and Jukka Tuhkuri. Velocity effects in laboratory scale punch through experiments. *Cold Regions Science and Technology*, 70, 81-93, 2012.

III Arttu Polojärvi, Jukka Tuhkuri and Otto Korkalo. Comparison and analysis of experimental and virtual laboratory scale punch through tests. *Cold Regions Science and Technology*, 81, 11-25, 2012.

IV Arttu Polojärvi and Jukka Tuhkuri. On modeling cohesive ridge keel punch through tests with a combined finite-discrete element method. *Cold Regions Science and Technology*, 85, 191-205, 2013.

Author's Contribution

Publication I: "3D discrete numerical modeling of ridge keel punch through tests"

The paper introduces 3D numerical modeling of non-cohesive ice rubble as discontinuous material, and presents virtual full-scale punch through experiments. The author implemented the numerical model, analyzed the results, and wrote most of the paper. Jukka Tuhkuri contributed to the paper by giving valuable comments and suggestions, and by assisting in the writing process.

Publication II: "Velocity effects in laboratory scale punch through experiments"

The paper presents the laboratory-scale punch through experiments conducted for the experimental part of the study and includes the results and analysis on the effect of the loading rate in laboratory-scale punch through experiments. The author designed the experiments together with Jukka Tuhkuri. Furthermore, the author analyzed the results and wrote most of the paper. Jukka Tuhkuri contributed to the paper by giving valuable comments and suggestions on the manuscript and by assisting in the writing process.

Publication III: "Comparison and analysis of experimental and virtual laboratory scale punch through tests"

The paper compares 3D discrete numerical model for non-cohesive rubble with laboratory-scale experiments, and includes further results and

analysis from the experimental part of the study. The author designed the experiments together with Jukka tuhkuri. Furthermore, the author implemented the numerical model, analyzed the results, and wrote the paper. Jukka Tuhkuri gave valuable comments and suggestions on the manuscript. Otto Korkalo implemented the motion tracking tool used in the experiments to investigate the rubble deformation.

Publication IV: "On modeling cohesive ridge keel punch through tests with a combined finite-discrete element method"

The paper introduces a technique for modeling ridge keel freeze bonds within the combined finite discrete simulations. Furthermore, the paper includes simulations of full-scale punch through tests on partly consolidated rubble. The author implemented the numerical model, analyzed the results, and wrote the paper. Jukka Tuhkuri contributed to the paper by giving valuable comments and suggestions.

1. Introduction

1.1 Background

Ice ridges are common and important features in Northern seas. Ridges are formed by compression and the shearing of sea ice as it is driven by wind and currents. Ridges typically have two distinct parts, which are shown in Fig. 1.1. The visible part above the waterline is called the sail and the underwater part the keel. The keel can be further divided into a consolidated layer, comprised of frozen water and ice blocks, and into ice rubble. The rubble can be a collection of loose ice blocks, in which case it is called non-cohesive. Anyhow, often the rubble is partly consolidated, that is, it consists of ice blocks bonded together by freeze bonds. As the rubble pile can be extensive in size, it can cause significant loads on marine structures and vessels used in winter navigation. To enable the safe design of these structures, research on the material properties of ice rubble is needed.

Punch through experiments are a commonly used method for testing ice

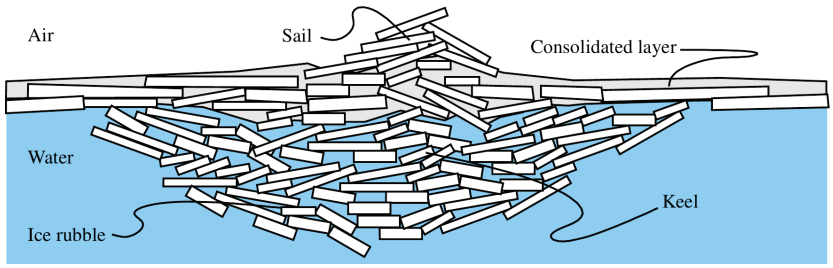

Figure 1.1. Cross section of a ridge, with its main parts indicated: The sail above the waterline and the keel underwater. The keel comprises of a consolidated layer close to the waterline and the unconsolidated, or partly consolidated, ice rubble. This rubble of ice blocks of the keel is of interest in this thesis.

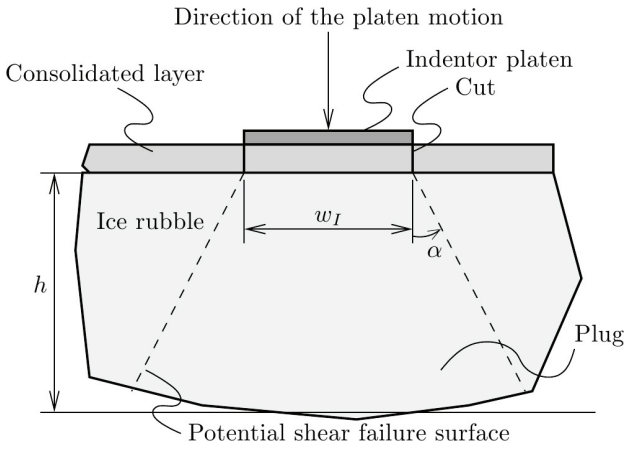

Figure 1.2. Sketch of the punch through test (reproduced from Heinonen (2004) with modifications). In the figure, an indentor with width w_I is loading ice rubble with depth h. A cut has been made through the consolidated layer to load the rubble only. In addition, a potential failure surface with angle α is shown, and a plug forming in the rubble failure is indicated.

rubble properties. It is an important testing method, because it is one of the only methods that can be used both, in full-scale and in a laboratory. Fig. 1.2 shows an illustration of a punch through experiment. In a punch through experiment, a flat indentor platen penetrates the rubble mass while the force applied by the rubble on the indentor is measured. The indentor force-displacement records, together with the dimensions of the experimental set-up, can then be used to derive material properties for the rubble. Deriving the material properties of the rubble from the experimental data is not a straightforward task, and numerical modeling is often needed to interpret the results of the experiments.

The first punch through experiments were performed by Leppäranta and Hakala (1989, 1992) in the Baltic Sea using a loading platform and concrete blocks. Since then, the experimental equipment has been improved and the method has been used in full-scale, as reported by, for example, Bruneau et al. (1998), Heinonen and Määttänen (2000, 2001a,b), Croasdale et al. (2001) and Heinonen (2004). Unfortunately, the possibilities to study the rubble behavior and its failure in the field are often limited.

Since a detailed study is needed to derive the material properties of the rubble, laboratory-scale experiments have been conducted by, for example, Leppäranta and Hakala (1992), Bruneau et al. (1998), Azarnejad et al. (1999), Azarnejad and Brown (2001), Jensen et al. (2001), Lemee

and Brown (2002) and Serré (2011). While the results from the laboratory tests have helped researchers understand the behavior of the rubble to a certain extent, the tests have also led to results that partly differ from the field experiments (Croasdale et al., 2001; Liferov and Bonnemaire, 2005). These differences include the loading rate dependencies of the rubble strength and failure mode (Azarnejad and Brown, 2001).

Modeling of the ice rubble related problems, including punch through tests, have previously been often performed using analytical soil mechanics models (Ettema and Urroz, 1989) and continuum models (Heinonen and Määttänen, 2001b; Liferov et al., 2002, 2003; Heinonen, 2004; Serré, 2011). While the continuum models have been successful in replicating punch through experiments in full-scale (Heinonen, 2004) and at a laboratory-scale (Liferov et al., 2002, 2003; Serré, 2011), they suffer from the disadvantage that potentially important details of the behavior of the rubble can be rendered out from the modeling results due to continuum description of the rubble. Even if the ice rubble consists of a multitude of ice blocks, it has remained unclear, whether there are enough ice blocks to describe the rubble as a continuum, and thus if the continuum models can be reliably used.

This motivates the use of a discontinuous approach, in which the rubble is modeled block by block, used here. When rubble is assumed to be discontinuous, its deformation becomes modeled through the displacements of the individual ice blocks within it. The ice blocks are assumed to interact through pairwise contacts, which cause their motion. It is believed that the discontinuous approach helps to provide more of an understanding of the phenomena behind ice rubble behavior. This understanding can then be used, not only to estimate ice loads or to plan future experiments, but also to further improve the still more commonly used continuum models.

1.2 Objectives and scope

This thesis consists of an experimental study on and simulations of punch through experiments. The scope of the experimental work was to study the punch through experiments as an experimental method and to gain an understanding of how to interpret the results of the experiment. The goal of the modeling was to develop numerical tools for modeling ice rubble as discontinuous material. The model was applied to a study of the punch

through experiments due their importance as a testing method for ice rubble properties. Briefly, the objectives of the study were as follows:

- To develop tools for discrete numerical modeling of ice rubble related problems in 2D and 3D, with the main focus on modeling punch through experiments;

- To conduct punch through experiments on non-cohesive rubble in order to investigate the experimental technique and compare the observations to earlier experiments with ice rubble;

- To analyze the experiments conducted on non-cohesive rubble parallel with the numerical model so as to validate the model and to gain a better understanding of how the punch through experiment results should be interpreted;

- To extend the model to include rubble cohesion due to freeze bonds and to study the punch through experiments on partly consolidated ice rubble using a discrete approach.

1.3 Research approach

The laboratory-scale experiments were conducted on rubble comprised of plastic blocks instead of ice. This was done to simplify the interpretation of the experiment results, and with the goal of studying the experimental technique. The experimental set-up was similar to the so-called small scale plane strain punch through experiments conducted by Azarnejad and Brown (2001), in which the loading rate dependency of the rubble strength was first observed.

The discrete element method (DEM) and the combined finite-discrete element method (FEM-DEM) were used for the modeling. DEM is a traditional way of modeling discontinuum and dates back to Cundall and Strack (1979). In DEM, the individual particles are assumed to be stiff, and their deformation is taken into account within interparticle contact models. DEM was used here in 3D modeling of the punch through experiments on non-cohesive rubble. FEM-DEM is a technique for including the deformation of the particles when modeling the discontinuum (Munjiza

et al., 1995; Munjiza and Andrews, 2000; Munjiza, 2004). In the work on 2D modeling of punch through experiments on partly consolidated rubble, the blocks within the keel were deformable and the material stress state at the freeze bonds was needed, thus FEM-DEM was used.

Numerical modeling of ice rubble related problems using DEM and FEM-DEM has been used earlier in studies on ice ridging (Hopkins, 1992, 1998; Hopkins et al., 1999), ice pile-up against structures (Paavilainen et al., 2006, 2009, 2011; Paavilainen and Tuhkuri, 2012; Haase et al., 2010) and punch through experiments on unconsolidated rubble (Tuhkuri and Polojärvi, 2005).

1.4 Structure of the thesis

This thesis first introduces the experimental work and results on the loading rate depended effects in the laboratory-scale punch through tests are presented (Publication II). After this, the numerical modeling is discussed and the key ingredients of all simulations within the thesis are described. Then, the results from the virtual punch through experiments are presented: first from the 3D DEM simulations on non-cohesive rubble done in laboratory (Publication III) and in full-scale (Publication I), and then from the 2D FEM-DEM simulations on partly consolidated rubble (Publication IV). Finally, the thesis concludes with a brief discussion on the main results and some remarks on future work.

2. Experimental study

2.1 Overview of the experiments

Laboratory scale punch through experiments were performed to study punch through experiments as an experimental method. Experiments were conducted on non-cohesive rubble comprised of plastic blocks. Plastic blocks were used to simplify the phenomena during the experiments by avoiding the bonding of the blocks due to, for example, freezing and sintering characteristic of the ice blocks (Kuroiwa, 1961; Ettema and Schaefer, 1986).

The emphasis of the study was on the effect of loading rate on punch through tests (Publication II) and on interpreting punch through indentor force-displacement histories (Publications II and III). The effect of loading rate was studied, as earlier laboratory-scale experiments with ice rubble (Azarnejad and Brown, 2001) have suggested, that an increase in indentor velocity causes a change in the rubble failure process and an increase in rubble shear strength. A study on the interpretation of slow punch through experiment results was performed with the aid of the numerical model, hence the results on this issue will be presented in Section 4.2.1 together with the simulation results.

2.2 Experimental set-up

The experimental set-up illustrated in Fig. 2.1 and described in detail in Publication II was similar to that used by Azarnejad and Brown (2001). The basin was made of transparent acrylic glass (PMMA) and was supported by a steel frame. The basin had two movable walls, which enabled to change its width w_b. The lateral force applied by the rubble on the in-

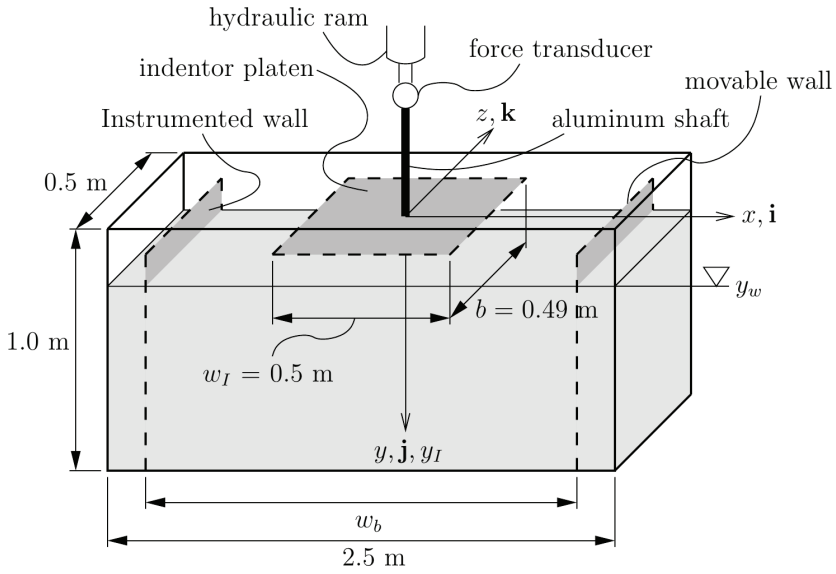

Figure 2.1. Experimental set-up used in the experiments in Publications II and III. The short walls at $x = \pm w_b$ of the basin were movable. The rubble blocks and the basin covers used in some experiments are not shown for clarity.

strumented movable wall at $x = -w_b/2$ was measured to investigate the lateral confinement within the rubble.

The indentor platen and the rubble blocks were made of polyethylene (PE). The blocks were homogeneous in size and cuboid in shape. Due to the material and force levels of the experiments, the deformation of the individual blocks and the indentor platen were negligible.

2.3 Experiment types

Two different types of punch through experiments were conducted: uncovered and covered basin experiments. The experiment types differed by the boundary conditions on the top of the rubble. In the covered basin experiments, the rubble beside the indentor platen was covered by PE-plates, whereas in the uncovered basin experiments these plates were not used.

The boundary conditions used here can be compared to those in the experiments with ice rubble. In the experiments performed on virtually non-cohesive ice rubble, the boundary conditions were similar to those of the uncovered experiments here. In contrast, in a punch through experiment on partly consolidated ice rubble, a layer of ice (ice sheet or consolidated

layer) covers the rubble (see Fig. 1.2). This layer is typically cut along the indentor platen perimeter to perform the experiment on ice rubble only, hence the boundary conditions are similar to those in the covered basin experiments.

In addition to the actual punch through tests, two types of reference experiments were conducted: open water and block experiments. In open water experiments, the indentor moved into the basin filled with water only. The block experiments were similar to the open water experiments, but in the block experiments a solid PE block was moving with indentor. The open water and block experiments were similar to those used by Azarnejad and Brown (2001), where the goal was to be able to take into account how much the experimental equipment and the rubble inertia contributed to the measured load records.

Indentor velocities $v_I = 2.5 \ldots 40$ mm/s were used. With the lowest velocities, a case of quasi-static loading was obtained and the effect of the water could be reliably analyzed, while with the highest velocities the hydrodynamic forces clearly affected the results. The velocities were not chosen after any full-scale ice rubble processes; they were chosen to study the experimental method. The test matrix can be found in Publication II.

2.4 Experiment results

In Publication II demonstrated that in the laboratory-scale punch through experiments, an increase in the rubble shear strength τ with an increase in the indentor velocity is likely partly due to the experimental set-up. The study in the paper was similar to analysis presented by Azarnejad and Brown (2001), and it was performed on uncovered basin experiments. To derive τ from the experimental data, a relation between the rubble resistance and the measured indentor force F_I records was first established as follows.

The force due to rubble resistance was achieved by subtracting the load components due to hydrodynamics and rubble buoyancy from measured F_I. The hydrodynamical force F_H was derived from the reference experiments, as presented below, and the buoyant load was estimated based on the residual force F_I^r measured at the end of each punch through experiment. Once these components had been derived using the respective experiments, the rubble shear strength τ was computed using the equa-

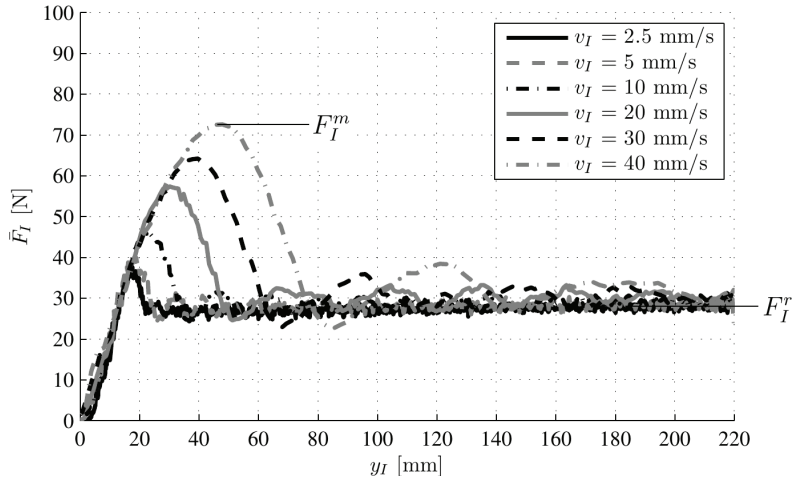

Figure 2.2. Indentor load from open water experiments with all of the indentor velocities v_I used: The mean indentor force $\bar{F}_I$ derived from repeated experiments as a function of indentor displacement y_I. A distinct peak yielding maximum load F_I^m (indicated for indentor velocity $v_I = 40$ mm/s), which occurred after the indentor platen water entry, is seen in all graphs. In addition, the figure shows the residual force F_I^r.

tion

$$\tau = \frac{F_I^m - F_I^r - F_H}{A}, \tag{2.1}$$

where A is area of the shear planes (see Fig. 1.2). Here, $A = 2hb$, where h is the rubble thickness and b the test basin width (see Fig. 2.1).

2.4.1 Reference experiments

The open water experiments used to achieve hydrodynamic force F_H in Eq. 2.1 were investigated in Publication II. The indentor load-displacement ($F_I - y_I$) records from these experiments are given in Fig. 2.2. The distinct peak in the $F_I - y_I$ curves of the figure, which also yielded the maximum load F_I^m, was due to the hydrodynamics after the indentor platen water entry. The residual load F_I^r after the peak in the open water experiments was mainly due to the buoyancy of the indentor.

The hydrodynamical force was defined based on the load records of the open water experiments as $F_H = F_I^m - F_I^r$ for each indentor velocity v_I. It was shown that F_H was not caused by stationary waves in the basin, but instead, that F_H was related to the flow of water on top of the indentor platen. The block experiments yielded very similar $F_I - y_I$ graphs as the open water experiments, with the distinction that the F_I levels increased by the block buoyancy.

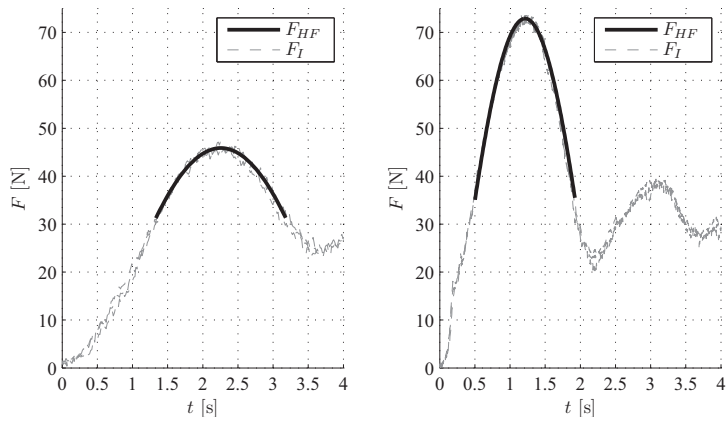

Figure 2.3. Fit F_{HF} shown on top of the indentor load records from three open water experiments with indentor velocities (a) $v_I = 10$ mm/s and (b) $v_I = 40$ mm/s.

For the analysis of F_I records from the actual punch through experiments with various loading rates, the fits F_{HF} for the peak resulting from F_H in the open water experiments were derived. Two examples of such fits are shown in Fig. 2.3 together with the $F_I - t$ records. These fits were then translated to align with the maximum load in the punch through test F_I records in order to analyze the hydrodynamical effects in the experiments as shown below.

In the case of the slow experiments, the analysis of the indentor force records was straightforward, since the contributions of the experimental set-up and hydrodynamics could reliably be taken into account, and the indentor load resulting from the rubble material only could be derived. This derivation is not discussed until Section 4.2.1, when the slow experiments are analyzed using the simulation results. However, the fast experiments are discussed below.

2.4.2 Effect of indentor velocity

The indentor velocity v_I was observed to drastically affect the experimental indentor force-displacement records and the derivation of the material properties of the rubble. It was concluded in Publication II that the rubble strength τ, defined from the data using Eq. 2.1, might be overestimated in the fast experiments. The reason for this is that the hydrodynamical force F_H used in Eq. 2.1 may differ between the open water and punch

through experiments due to the experimental set-up, as described in the following.

The effect of v_I on the punch through experiment results is clearly illustrated by comparing Figs 2.4 a and b, which show F_I records from a slow and fast experiment: F_I^m occurred later and clearly had higher value in the fast experiment compared to the slow experiment. In addition to the $F_I - y_I$ records, Fig. 2.4 shows the fit F_{HF} for hydrodynamical force. The peak in the experiments was related to hydrodynamics: In the case of the slow experiment (Fig. 2.4a), it was observed that the F_{HF} provides a good estimate of the peak in the F_I record, whereas in the case of the fast experiment (Fig. 2.4b), the F_{HF} still has approximately same shape as the peak in F_I record. Anyhow, in Publication II it was shown that the peak load F_I^m in the punch through experiments increased clearly more strongly with v_I than F_H or F_I^m in the open water experiments. To demonstrate a reason for this, two sequences of snapshots from the slow and the fast experiment leading to the force records in Figs 2.4 a and b, respectively, are shown in Fig. 2.5.

As mentioned above, F_I^m occurred at higher indentor displacement in fast (instance (2b) in Fig. 2.4b and 2.5b) than in the slow experiment (instance (1a) in Fig. 2.4a and 2.5a). The occurrence of F_I^m in the fast experiments was accompanied by a rapid flow of water through the rubble mass towards the indentor center line, with the rubble restricting the flow. As simultaneously the movement of the rubble blocks over the indentor platen was obstructed by the indentor platen itself, the force needed to enable the flow is higher than in the open water experiments. The indentor platen obstructing the movement of the rubble blocks with the water likely leads to an increase in the F_I^m, not only due the rubble properties and F_H from the open water experiments, but also due to the set-up of the experiment. After (2b) in the fast experiment, the rubble started to move over the indentor as indicated by the arrows marked with (A) in Fig. 2.5 (3b). This movement of the rubble started immediately after the F_I^m was reached and continued during the fast decrease in the F_I records up to (3b) in Fig. 2.4b, after which more stationary force levels were reached.

The effect of indentor velocity v_I on rubble shear strength τ given by Eq. 2.1 was discussed in Publication II. The τ values that were derived increased with the loading rate analogously to ice rubble in similar tests. As the observations above showed, the hydrodynamical force, F_H, in the open water experiments may be different than in the punch through ex-

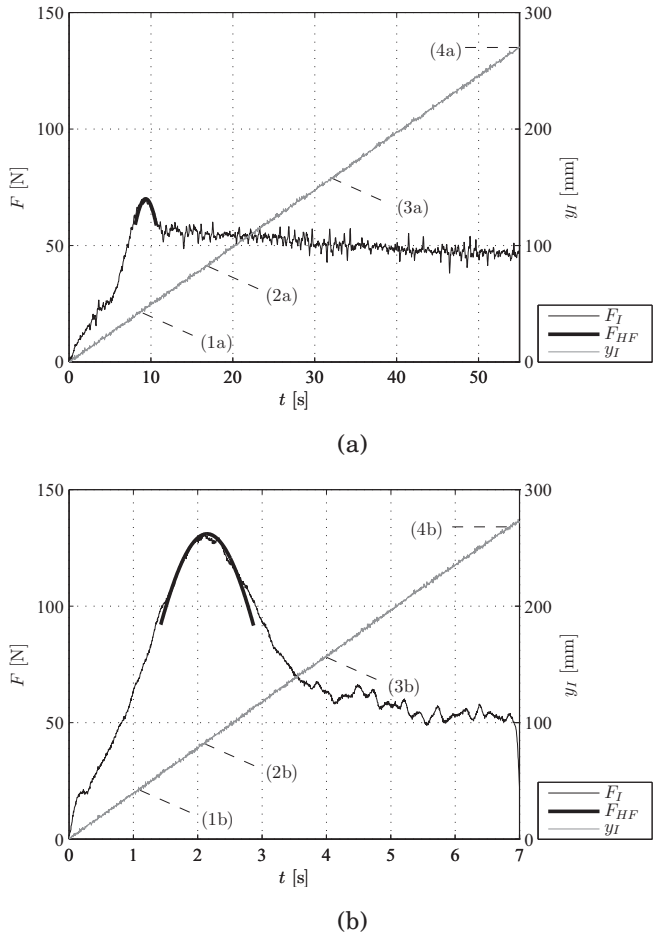

Figure 2.4. The F_I records for the punch through experiments shown in a sequence of snapshots in Fig. 2.5: (a) Indentor velocity $v_I = 5$ mm/s and (b) $v_I = 40$ mm/s. The markers in the figures correspond to the snapshots in Fig. 2.5. F_{HF} in the figure refers to the hydrodynamic force from the open water experiments and y_I is the indentor displacement.

periments. Hence, it was concluded that the loading rate dependency of the rubble shear strength, τ, observed in the laboratory experiments can be at least partially caused by the experimental set-up instead of the rubble material.

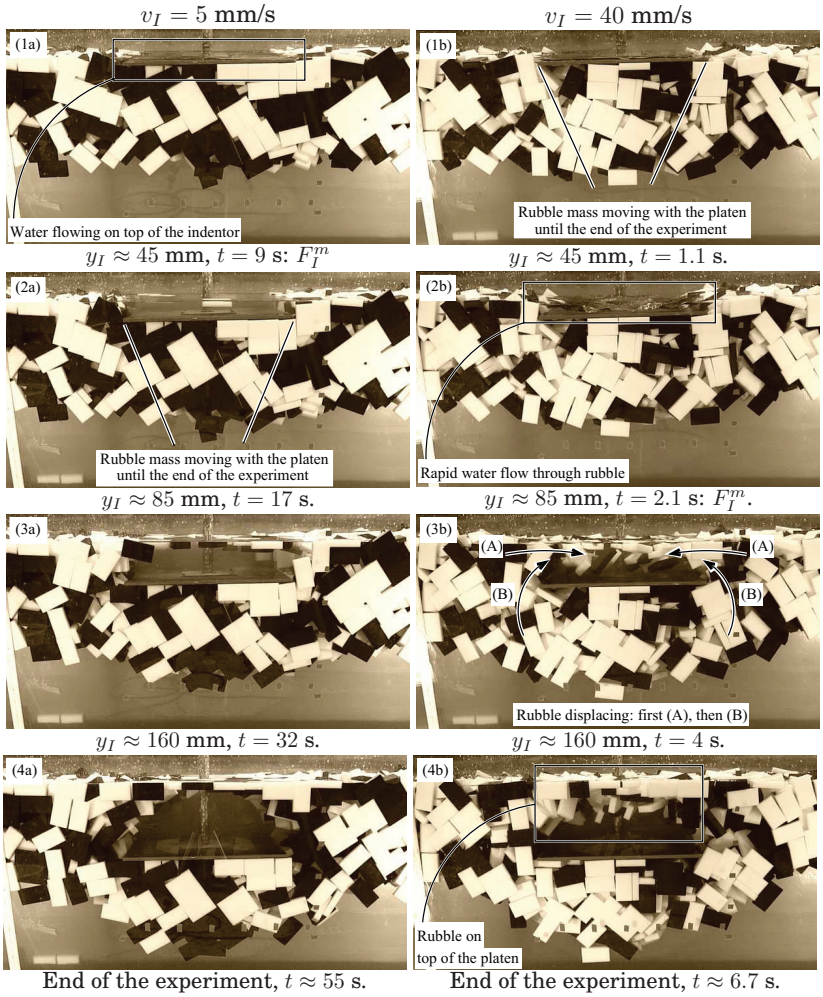

Figure 2.5. Sequences of snapshots from the experiments with $v_I = 5$ mm/s (left column) and $v_I = 40$ mm/s (right column) with four different indentor displacements y_I. The instance of maximum indentor force F_I^m for both experiments is indicated under the corresponding figure. The indentor force F_I records these experiments are given in Fig. 2.4.

3. Mechanics of the simulations

3.1 Overview of the simulations

The simulations were performed using the 3D discrete element method (DEM) (Publications I and III) and the 2D combined finite-discrete element method (FEM-DEM) (Publication IV). In both techniques, the discrete elements representing the rubble blocks were meshed into finite elements. In FEM-DEM, the finite elements were used to solve the block deformation and contact forces between the contacting blocks, whereas in DEM they were only used to solve the contact forces. All simulations were explicit.

On each time step in the 3D DEM simulation, the following four tasks were performed: (1) The neighbor search for potentially contacting blocks, (2) derivation of contact forces, (3) adding external forces and (4) updating positions. For task (1), the algorithm presented by Munjiza and Andrews (1998) was used with some modifications to find the potentially contacting blocks.

In 2D simulations with deformable blocks and freeze bonds, the additional three tasks were (1) to determine the internal forces according to the displacement field for continuous material, (2) to check the stress state at the freeze bonds and (3) to compute the cohesive forces at the freeze bonds under failure process.

3.2 Contact forces

In all simulations, the contact forces were derived using penalty function and potential contact force method (Munjiza et al., 1995; Munjiza and Andrews, 2000; Munjiza, 2004). In the potential contact force method, a

potential φ with continuous first partial derivatives with respect to spatial coordinates is defined in every point P of each finite element area (element volume in 3D) Γ. Furthermore, $\varphi = \varphi(P)$ should vanish at finite element boundary S for a smooth collision response. In the case of triangular (2D) or tetrahedron (3D) shaped finite elements, the obvious choices for $\varphi(P)$ are the area or volume coordinates, respectively.

The contact force $\mathrm{d}\mathbf{f}_\varphi$ applied to an infinitesimal area (volume) element $\mathrm{d}\Gamma_o$ penetrating into φ was determined from the gradient of φ as (Fig. 3.1a)

$$\frac{\mathrm{d}\mathbf{f}_\varphi(P)}{\mathrm{d}\Gamma_o} = -s\nabla\varphi(P), \tag{3.1}$$

where s is a positive constant penalty term. The value of s controls the amount of penetration the contacting blocks in the simulation can have. Here, the value of s was chosen high enough to virtually avoid contacting blocks from overlapping. Further, it was ensured that further increase in its value would not have a major effect on the simulation results. It should also be noted that there is no specific value to assign for s, since no analytical contact law for arbitrarily shaped polygonal (polyhedral) particles exists.

The contact force $\mathbf{f}_\varphi$ resulting from $\varphi(P)$ was determined by integrating over the overlap area (volume) Γ_o of two colliding elements. The integral was reduced to a computationally more efficient integral over the boundary $\mathrm{d}\Gamma_o$ by using a generalized version of Gauss's theorem

$$\mathbf{f}_\varphi = -s\int_{\Gamma_o} \nabla\varphi(P)\ \mathrm{d}\Omega = -s\int_{S_o} \varphi(P)\mathbf{n}\ \mathrm{d}\Gamma, \tag{3.2}$$

where $\mathbf{n}$ is the unit outer normal of S_o (Fig. 3.1b). Here, as triangular (2D) or tetrahedron (3D) shaped finite elements were used, boundary of S_o consisted of lines (2D) or triangular (3D) surfaces. Hence, the previous integral could be solved in parts (each part consisted of a line or a surface), with each part having a constant normal $\mathbf{n}$. For each part, a force system equivalent to that given by Eq. 3.2 for the part was computed and applied to the vertices of the line or a surface belonging to that part.

The inelasticity in collisions of rigid blocks in 3D DEM simulations in Publications I and III was achieved by viscous damping relative to the rate of change in the overlap volume. The viscous component of the normal force $\mathbf{f}_v$ was defined as

$$\mathbf{f}_v = c\Gamma_0\,(\mathbf{v}_r \cdot \mathbf{n})\,\mathbf{n}, \tag{3.3}$$

where $\mathbf{v}_r \cdot \mathbf{n}$ is the normal component of the relative velocity of the contacting blocks at the point of application of $\mathbf{f}_\varphi$ and c is the viscous damp-

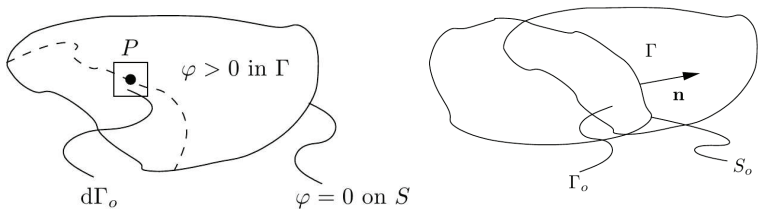

Figure 3.1. (a) An infinitesimal area element $\mathrm{d}\Gamma$ at point P penetrating a finite element with area Γ and (b) the overlap area $\mathrm{d}\Gamma_o$ of two elements.

ing constant. No tensile forces between colliding blocks were allowed and thus the total contact force $\mathbf{f}_c$ should always act on the direction of $-\mathbf{n}$ when contacts occur. Hence, the following condition was used:

$$\mathbf{f}_c = \begin{cases} 0, & \text{if } |\mathbf{f}_\varphi| - |\mathbf{f}_v| < 0 \\ \mathbf{f}_\varphi - \mathbf{f}_v & \text{else.} \end{cases} \tag{3.4}$$

For the FEM-DEM simulations using deformable blocks, discussed in Publication IV, no viscous damping in contact forces was needed, as the damping was due to the energy dissipation related to the deformation of the solid blocks.

In all simulations, dissipation due to sliding friction was modeled using dynamic Coulomb friction. Frictional force $\mathbf{f}_\mu$ was solved using the following equation:

$$\mathbf{f}_\mu = -\mu|\mathbf{f}_c|\frac{\mathbf{v}_r - \mathbf{v}_r \cdot \mathbf{n}}{|\mathbf{v}_r - \mathbf{v}_r \cdot \mathbf{n}|}, \tag{3.5}$$

where μ is the friction coefficient and $\mathbf{v}_r - \mathbf{v}_r \cdot \mathbf{n}$ is the tangential component of the relative velocity of contacting blocks at the point of contact.

3.3 Freeze bonds

The freeze bonds for partly consolidated rubble in Publication IV were modeled using initially rigid cohesive elements (Camacho and Ortiz, 1996; Ortiz and Pandolfi, 1999; Sam et al., 2005; Morris et al., 2006; Block et al., 2007). In this approach, an initially continuous finite element mesh can undergo energy dissipating cohesive fracture process on its parts fulfilling a failure criterion. The approach was used here, as Fig. 3.2 illustrates: The simulated keel was meshed in its initial configuration, with the mesh being continuous over the contacting surfaces of the blocks.

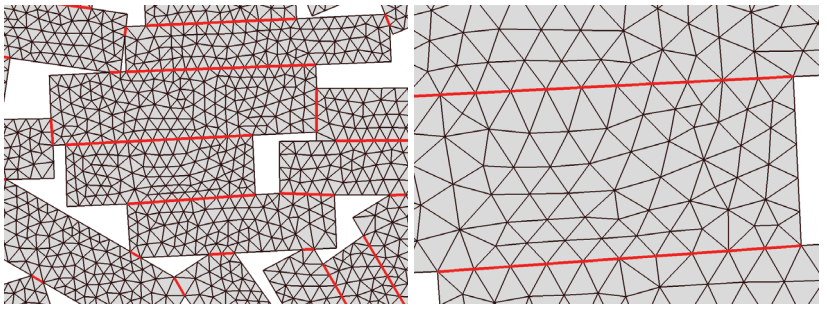

(a) (b)

Figure 3.2. Two snapshots from a simulation: (a) Ice blocks bonded together by freeze bonds (red) and (b) a close-up of two freeze bonds.

As Fig. 3.2 further shows, the finite element edges connecting the blocks were defined as freeze bonds and thus potential sites for failure. On each time step of a simulation, the stress state at each freeze bond point (a finite element mesh node belonging to a freeze bond) was monitored and compared to a failure criterion. The failure criterion used for the freeze bonds is

$$t_e \geq \sigma_{cr}, \tag{3.6}$$

where t_e is the effective traction at a bond point and defined as

$$t_e = \begin{cases} \sqrt{\beta^{-2} t_t^2 + t_n^2} & \text{if } t_n \geq 0 \\ \beta^{-1}(|t_t| - \mu |t_n|) & \text{if } t_n < 0. \end{cases} \tag{3.7}$$

In the definition of t_e, t_t and t_n are the tangential and normal components of the traction vector $\mathbf{t}$ at a bond point, respectively, whereas μ is the friction coefficient. Furthermore, β is the shear stress factor, defined as $\beta = \tau_{cr}/\sigma_{cr}$, where τ_{cr} and σ_{cr} are the shear and tensile strengths of the bond, respectively.

Once the failure criterion at a freeze bond point was reached, the point underwent a cohesive crack growth process. When cohesive crack growth at a freeze bond point was initiated, the finite element mesh node was split into two nodes with initially equal nodal coordinates $\mathbf{x}^+$ and $\mathbf{x}^-$, as shown in Figs. 3.3a and b. Mass m of the node before splitting was divided to the new nodes according to the elements connected to the node, hence $m^+ + m^- = m$.

During the cohesive crack growth process, a nodal cohesive force $\mathbf{f}_c = \mathbf{f}_c^+ = -\mathbf{f}_c^-$ that resists the cohesive crack opening is applied to the newly generated nodes in a manner similar to that of Block et al. (2007). The

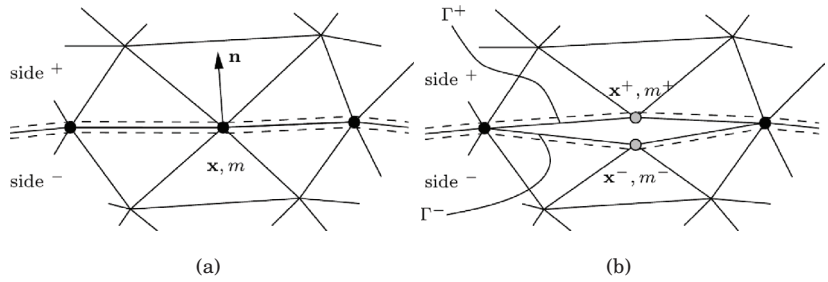

Figure 3.3. An illustration of the bond splitting: (a) An intact node belonging to the bond surface (between dashed lines) with normal $\mathbf{n}$, nodal coordinate $\mathbf{x}$, and mass m is have been splitted into (b) two nodes with masses m^+ and m^- and nodal coordinates $\mathbf{x}^+$ and $\mathbf{x}^-$. Similarly, new crack surfaces Γ^+ and Γ^- have been generated.

initial value $|\mathbf{f}_c^0|$ is derived as follows. The elements connected to node $^{+(-)}$ are used to compute the internal force vector $\mathbf{f}^{+(-)}$ for the stress state $t_e = \sigma_{cr}$ (Eq. 3.6). Then, $\mathbf{f}^{+(-)}$ are used to solve the initial value $|\mathbf{f}_c^0|$ (Papoulia and Vavasis, 2003; Sam et al., 2005; Block et al., 2007):

$$|\mathbf{f}_c^0| = \left| -\frac{m^-}{m}\mathbf{f}^+ + \frac{m^+}{m}\mathbf{f}^- \right|. \tag{3.8}$$

As the distance between the nodes $^-$ and $^+$ increases during the crack growth, the value of the cohesive force $|\mathbf{f}_c|$ decreases following the linear softening law illustrated in Fig. 3.4. As the figure shows, $|\mathbf{f}_c|$ is a function of effective crack opening displacement (Camacho and Ortiz, 1996; Ortiz and Pandolfi, 1999; Sam et al., 2005)

$$\delta_e = \sqrt{\beta^2\delta_t^2 + \langle\delta_n\rangle^2}, \tag{3.9}$$

where δ_t and δ_n are the components of the cohesive crack opening displacement $\boldsymbol{\delta} = \mathbf{x}^+ - \mathbf{x}^-$ in tangential and normal directions of the freeze bond, respectively. The operator $\langle\rangle$ in the definition is the Macaulay brackets; hence, $\langle\delta_n\rangle = 0$ if $\delta_n < 0$.

The cohesive crack growth can include loading, unloading and reloading phases, as illustrated in Fig. 3.4: δ_e increases in the loading phase, it decreases in unloading phase, it increases again during the reloading phase; but has a value smaller than the maximum effective crack opening displacement δ_m reached during the preceding loading phase. The irreversibility of this crack growth process is ensured by solving the cohesive

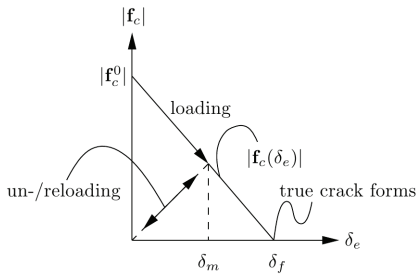

(a)

Figure 3.4. Linear softening function $\mathbf{f}_c(\delta_e)$ and the crack opening, unloading and reloading phases of cohesive crack growth. In the figure, δ_e is the effective crack opening displacement defined in Eq. 3.9, δ_m is the maximum crack opening displacement reached during loading phase and δ_f is the critical crack opening displacement.

force value during these phases based on the following equation:

$$|\mathbf{f}_c|(\delta_e) = \begin{cases} |\mathbf{f}_c^0| \left(1 - \dfrac{\delta_e}{\delta_f}\right) & \text{in loading} \\ |\mathbf{f}_c^0| \left(1 - \dfrac{\delta_m}{\delta_f}\right) \dfrac{\delta_e}{\delta_m} & \text{in un-/reloading.} \end{cases} \tag{3.10}$$

The direction of the cohesive force depends on components δ_t and δ_n of cohesive crack opening displacement $\boldsymbol{\delta}$. Using these, the tangential and normal components of the cohesive force are, respectively, solved from

$$f_{ct} = |\mathbf{f}_c|(\delta_e) \left(\frac{\beta\delta_t}{\delta_e}\right) \qquad \text{and} \qquad f_{cn} = |\mathbf{f}_c|(\delta_e) \left(\frac{\langle\delta_n\rangle}{\delta_e}\right). \tag{3.11}$$

As Fig. 3.4 further shows, $|\mathbf{f}_c(\delta_e)|$ linearly decreases with an increasing δ_e and vanishes once δ_e reaches δ_f. The value of δ_f is not a material parameter, but instead is derived from the fracture energy G: If the length of the newly formed crack surfaces associated with a bond point is l, then the energy dissipated due to cohesive crack growth process at the point should be equal to Gl in 2D. Using the definition of work and the linear softening law illustrated in Fig. 3.4, and requiring the dissipation in cohesive crack growth process to be equal to Gl, the value of δ_f is achieved from the following equation:

$$\int_0^{\delta_f} |\mathbf{f}_c\,(\delta_e)|\,d\delta = \frac{1}{2}\,|\mathbf{f}_c^0|\,\delta_f = Gl \qquad \Rightarrow \qquad \delta_f = \frac{2Gl}{|\mathbf{f}_c^0|}. \tag{3.12}$$

3.4 Deformation

In the FEM-DEM simulations, discussed in Publication IV, the ice blocks were deformable. The deformation of the continuous ice blocks was as-

sumed to be small, while large displacements of individual blocks were allowed. The material behavior of the continuous ice blocks was linear elastic, as instead of the deformation of the individual ice blocks, the deformation of ice rubble is dominated by interparticle sliding and movement of the blocks within the rubble (Sayed et al., 1992).

Furthermore, the material behavior of the blocks was assumed to be isotropic, and plane strain state was assumed. The material damping of the blocks on elastic regime was viscous. The internal forces resulting from the deformation of the blocks were solved using constant strain triangle elements; the solution procedure was implemented as presented in detail in Munjiza (2004).

3.5 External forces

Determining the buoyant force due to the water and the gravitational force acting on the blocks in the 3D simulations was fairly straightforward and is described in Appendix A of Publication III. The gravitational acceleration could be directly applied on the block centroids according to the masses of the blocks. Similarly, the buoyant force for the submerged blocks could be applied on block centroids using the material densities of the blocks and water. For partly submerged blocks, the buoyant force was applied by integrating hydrostatic pressure over the surfaces of the submerged parts of the blocks. In the case of the 2D FEM-DEM model (Publication IV), gravitational and buoyant forces were applied as body forces.

Rigorous modeling of the hydrodynamical forces acting on the rubble blocks was not attempted in any of the simulations. Anyhow, a simplified model for the water drag acting on the blocks was implemented in Publication III. The model was derived to approximate pressure drag on the blocks, as described in Appendix A of the paper. As only the punch through experiments with slow indentor velocities were modelled in this work, the use of the approximation for the hydrodynamical forces presented in Publication III is believed to be justified.

4. Virtual punch through experiments

4.1 Overview of the virtual experiments

Virtual experiments were reported in Publications I, III and IV. In Publications I and III, the rubble was non-cohesive and a 3D discrete element method was used. In Publication IV, the rubble was partly consolidated and a 2D combined finite-discrete element method was applied in modeling. A model for the freeze bonds for partly consolidated rubble was presented in Publication IV.

4.2 Non-cohesive rubble

4.2.1 Laboratory scale

In Publication III, the 3D DEM model was successfully validated by modeling slow laboratory-scale experiments. The model was then used to analyze of the experiments. The need for a numerical model to correctly represent the rubble deformation throughout the experiment was demonstrated, as a clear relation between the deformation patterns and load records was found. The simulations were performed using rigid blocks with the shape, size and mass properties chosen after the experiments, and the simulation domain had the dimensions of the test basin shown in Fig. 2.1. Typical initial configurations for simulations of different punch through experiment types (see Section 2.3) are shown in Fig. 4.1. The simulation parameters can be found in Publication III.

Based on the experimental results, indentor load records resulting only from the rubble material (F_R) could be reliably defined for the slow exper-

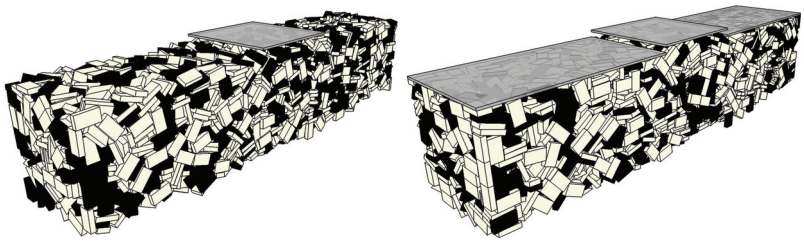

(a) (b)

Figure 4.1. Virtual punch through experiments before indentor motion: Simulation of (a) an uncovered and (b) a covered basin experiment. The domain for the simulations was chosen according to the test basin illustrated in Fig. 2.1 (the basin walls are not shown here for clarity).

iments. Fig. 4.2 shows how the F_R records for the slow experiments could be derived: the indentor force records from open water experiment were subtracted from those of the punch through experiment. The simulations and experiments yielded very similar F_R records. This is shown by the mean rubble load records $\bar{F}_R$ (the rubble load records derived using the load histories from number of repeated simulations and experiments) in Figs 4.3 a and b: In all simulations and experiments, $\bar{F}_R$ increased at the same rate in the beginning of the indentor penetration and reached its maximum with an approximately equal indentor displacement. In addition to the F_R records, the maximum rubble load F_R^m values with various rubble thicknesses were in good agreement. The basin width w_b had only a negligible effect on the F_R records and the F_R^m values.

The deformation patterns in the experiments were analyzed using video recordings and motion tracking software, as described in Publication III. In the analysis, the amount of rubble displaced by ratio R of the indentor displacement y_I could be detected from the videos and was used to visualize the rubble deformation fields. A similar analysis was performed on the simulation data, and a good agreement between the deformation patterns in the experiments and the simulations was found.

The snapshots in Fig. 4.4 demonstrate the analysis and the similarity of the deformation patterns in the experiments and simulations. In the first snapshot, with the indentor displacement $y_I = 35$ mm, the indentor platen has reached the water surface and a wedge-shaped volume of rubble under the indentor is moving downwards with it (area limited by red triangle in the figure). The next snapshot, with $y_I = 80$ mm, shows the deformation patterns at the maximum rubble load F_R^m. It can be noticed that the volume of displaced rubble has increased compared to the

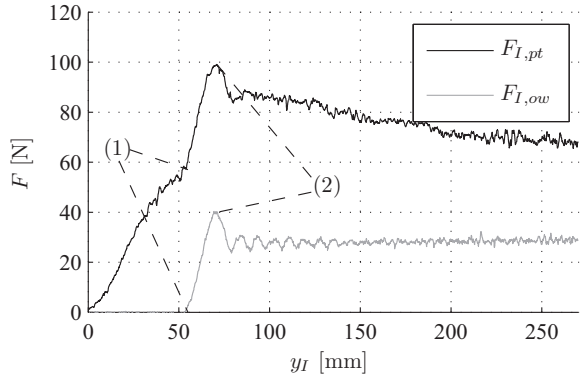

(a)

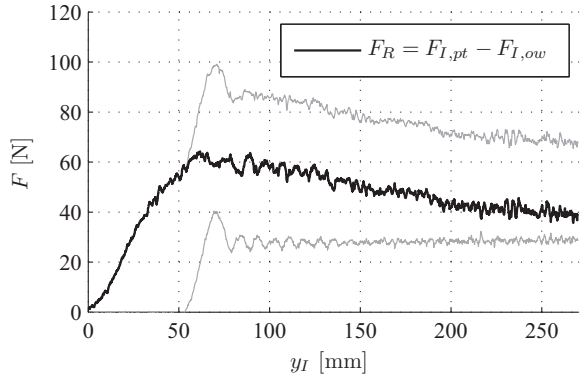

(b)

Figure 4.2. Definition of the rubble load F_R in slow laboratory-scale experiments: (a) Indentor load records from a punch through ($F_{I,pt}$) and an open water ($F_{I,ow}$) experiment with the same indentor velocity and (b) rubble load $F_R = F_{I,pt} - F_{I,ow}$. In (a), the indentor starts its entry into the water at (1) and the peak related to the hydrodynamic force occurs at (2), after the indentor submergence. In (b), $F_{I,pt}$ and $F_{I,ow}$ from (a) are shown in gray.

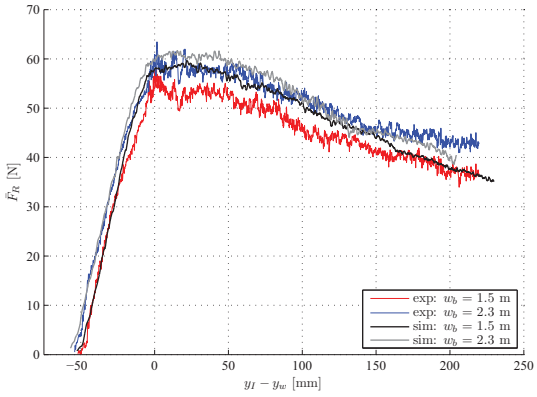

(a)

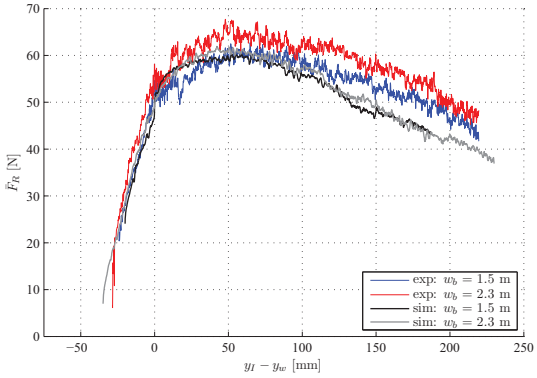

(b)

Figure 4.3. The mean rubble load $\bar{F}_R$ records from the experiments and the simulations: (a) Uncovered and (b) covered basin. $\bar{F}_R$ records from the experiments and simulations with a rubble thickness of 0.5 m and both basin widths w_b are shown. The x-axis shows the indentor position y_I in relation to the water surface y_w.

previous snapshot.

The simulation data was used to analyze the relation between the F_R records and the rubble deformation patterns in more detail, as the analysis was not limited only to the part of the rubble visible to the video camera. Results of this analysis are illustrated in Fig. 4.5. The figures show the total volume of blocks, with their centroids having downward velocities of $v_y > 2$ mm/s, $v_y > 5$ mm/s, and $v_y > 9$ mm/s in simulations with an indentor velocity of $v_I = 10$ mm/s.

Fig. 4.5 shows two distinct features concerning F_R records: The experiment type has an effect on the evolution of the displacing rubble mass, and that the volume of displacing rubble increases when the load F_R in Fig. 4.3b increases. Due to the fact that the downward-moving rubble volume increases during a longer displacement interval in the covered than in the uncovered basin experiments, the maximum rubble load is reached later in the covered experiments. As Figs 4.3 and 4.5 further show, the load F_R and the volume of solid material moving downwards decreased in all simulations towards the end of the indentor stroke.

As mentioned above, the lateral force F_x applied by the rubble on one of the short basin walls (see Fig. 2.1) was also measured in the experiments. Similarly to the experiments, the force F_x applied by the rubble on the short basin walls was gauged in the simulations. The F_x records yielded by the simulations were similar to those in the experiments. The increase in F_x during the indentor stroke was clear: With a basin width $w_b = 1.5$ m ($w_b = 2.3$ m), F_x increased on average 63% (51%) from its initial value.

The effect of an increasing F_x on the assessment of rubble material properties was discussed in Publication III. The increase in F_x was assumed to indicate an increase in confining pressure σ within the rubble. The Mohr-Coulomb material model was considered in the discussion. The Mohr-Coulomb model gives the following relation between the rubble shear strength τ, cohesion c, and internal friction angle ϕ:

$$\tau = c + \sigma \tan \phi. \tag{4.1}$$

The observed approximate 50 % increase in F_x, if not properly taken into account when deriving the material properties from the punch through experiment results, was shown to potentially lead to a severe overestimation of ϕ.

Also, the effect of the boundary conditions on the material modeling was discussed. It was shown that the maximum load due to rubble material (F_R^m) does not necessarily occur simultaneously with the measured

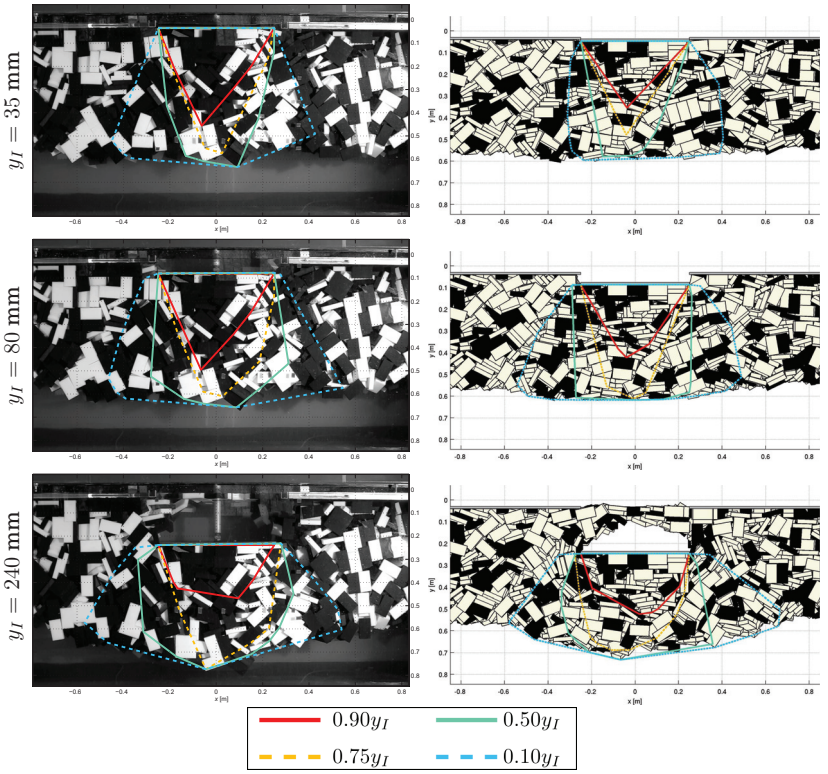

Figure 4.4. The deformation patterns with increasing indentor displacement y_I in a covered basin experiment (left) and a corresponding simulation (right). The displacement values Ry_I for the areas shown in the figure are given in the legend.

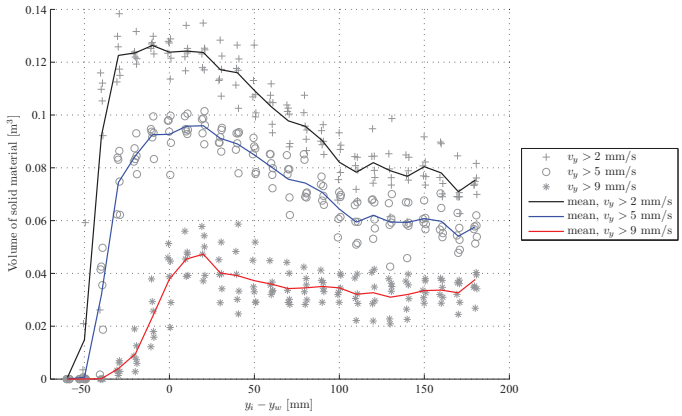

(a)

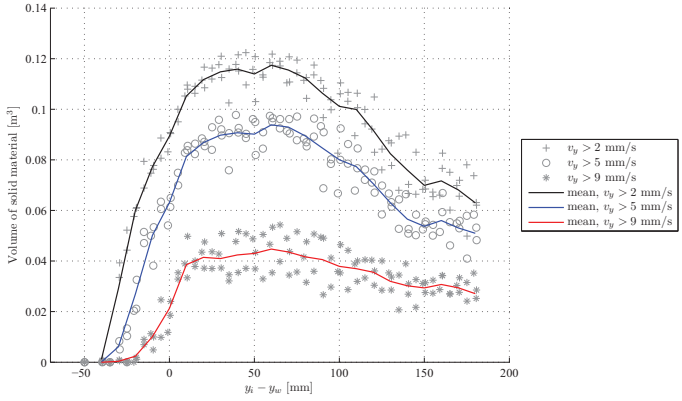

(b)

Figure 4.5. The volumes of the blocks moving downwards with velocities $v_y = 9, 5$ and 2 mm/s in simulated experiments with an indentor velocity of $v_I = 10$ mm/s: (a) Uncovered and (b) covered basin simulations.

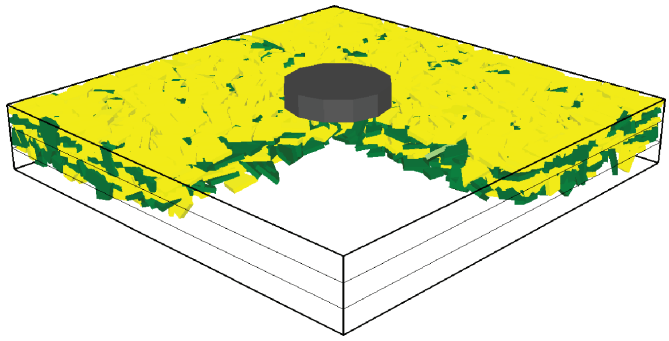

Figure 4.6. Typical initial configuration of the simulation in Publication I. The ice blocks at one quarter of the pool and the ice sheet covering the pool are not shown in the figure for clarity.

maximum indentor load (F_I^m): First was closely related to the rubble deformation, whereas the latter was related to the hydrodynamics (see (2) in Fig. 4.3a). As a result, interpreting the experimental records could be challenging, if the rubble deformation patterns are not known.

4.2.2 Full-scale

Full scale punch through experiments on non-cohesive rubble were simulated and analyzed in Publication I. The effect of friction on rubble resistance and the relation of the evolution of the rubble deformation patterns to indentor force records were studied. The simulations were conducted using the same 3D DEM code as was used to model the laboratory-scale tests above. In the simulations, the indentor platen was round, the rubble was covered by an ice sheet, and the domain was fully 3D, as illustrated by Fig. 4.6. Publication I gives a detailed description of the set-up for the simulations and a table of the parameters used in them.

Fig. 4.7 shows typical indentor load displacement ($F_I - y_I$)[1] graphs from three different simulations with the same initial configuration but with different values for the friction coefficient μ. As shown by the figure, initially the F_I increased steeply until it reached an approximately constant level. As in the case of slow laboratory experiments and the simulations of them described above, the $F_I - y_I$ records were related to the rubble deformation patterns.

The rubble deformation was analyzed using angle α_t, which was an ap-

[1]The symbols from Publication I have been changed here to match the notation used in earlier text. The following substitutions were made: $\delta \rightarrow y_I$, $F \rightarrow F_I$, and $F_{MAX} \rightarrow F_I^m$.

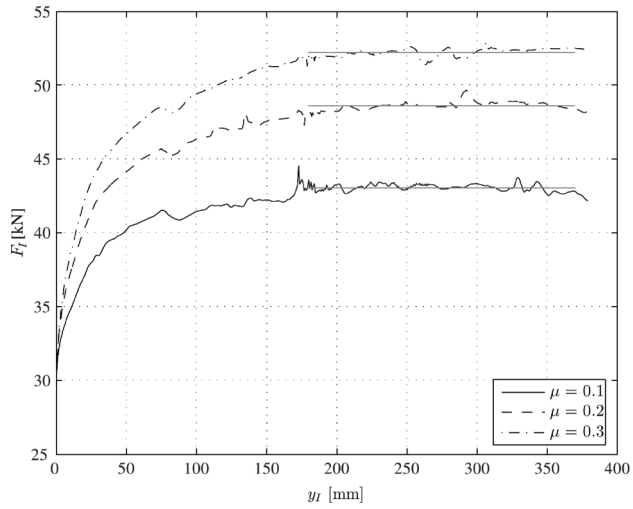

Figure 4.7. Indentor force-displacement ($F_I - y_I$) records from the simulations of full-scale experiments on non-cohesive rubble with three different friction coefficients μ. The maximum load F_I^m was defined as the average of F at an approximately constant level, which is shown with gray line for each plot.

proximation of shear plane angle α in Fig. 1.2. Essentially, α_t was the slant angle of the truncated cone enclosing the volume of displacing rubble under the indentor. The angle α_t was not constant during the indentor motion, as Fig. 4.8 shows. The value of α_t was related to the $F_I - y_I$ records as shown by the comparison of Figs 4.7 and 4.8: With a small y_I, the rate $\partial\alpha_t/\partial y_I$ was high, similarly to the rate $\partial F_I/\partial y_I$ of the increasing indentor load. Hence, an increase in the F_I at the start-up of the virtual experiments was related to the evolution of the rubble deformation patterns. It was also concluded that a major part of the indentor load was due to the buoyancy of the rubble.

The failure process of the rubble was divided into three main parts: (1) A volume of rubble with the shape of an upward opening cone forms under the indentor, moves with the indentor, and spreads out into a cylindrical plug, (2) ice blocks around this conical/cylindrical core rotate (or shape lock and rotate), causing the zone of displaced rubble to spread horizontally, that is, the angle α_t defining a downward opening cone containing moving rubble grows, until (3) α_t reaches an approximately constant value and the rubble within the cone defined by α_t moves downwards.

The rubble shear strength τ was derived using the maximum force values F_I^m defined in Fig. 4.7. In Publication I, the τ values were derived simply by dividing the F_I^m with the area of the cylindrical failure surface

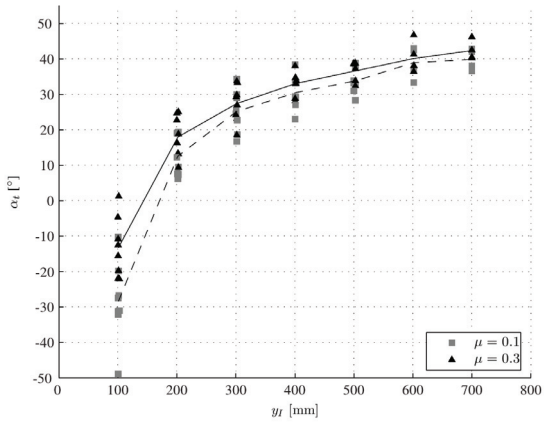

Figure 4.8. Angle α_t used to approximate the volume of displaced rubble as a function of indentor displacement y_I in simulated full-scale experiments.

(see Fig. 1.2 and assume that the indentor is round and that $\alpha = 0°$). The rubble τ increased in the simulations with friction coefficient μ: As μ was increased from 0.1 to 0.3, τ increased by approximately 20 %. The rubble porosity, defined as the ratio of empty space to the total rubble volume, appeared to be inversely proportional to the rubble shear strength.

The deformation patterns in the simulations were compared to laboratory-scale experiments and found to be in agreement: Angle α_t in Fig. 4.8 describing the volume of disturbed rubble reached values of up to approximately $40°$, which is close to that observed in laboratory by Jensen et al. (2001) and Lemee and Brown (2002). Furthermore, the maximum load values and the load records from the simulations were in fair agreement with a field experiment by Heinonen and Määttänen (2001c) on unconsolidated rubble.

4.3 Partly consolidated rubble

Punch through experiments on partly consolidated ice rubble were modeled and the effect of freeze bonds on the results of the experiments was discussed in Publication IV. It was shown that the buoyant load resulting from the rubble becoming detached from the surrounding rubble field and displacing during an experiment, is of crucial importance when interpreting the experiment results. In the simulations, a 2D combined finite-discrete element method was used with deformable ice blocks. The freeze bonds were implemented as described in Section 3.3. An illustra-

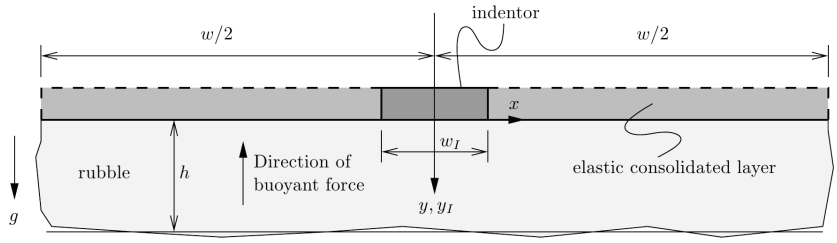

Figure 4.9. Simulation domain and boundary conditions in 2D FEM-DEM simulations on partly consolidated rubble. The upper boundaries of consolidated layer (marked with dashed lines) had a rigid boundary condition. The symbols in the figure are as follows: h is the rubble thickness, w the domain width, y_I the direction of indentor penetration, and g the gravitational acceleration. The axes (x, y) of the global coordinate system are also shown in the figure.

tion of the simulation set-up is given in Fig. 4.9. A detailed description of the simulations, together with the simulation parameters, can be found in Publication IV.

The typical features observed in simulations can be described using the indentor force-displacement $(F_I - y_I)$[2] records in Fig. 4.10. Initially, the F_I increased with a high rate, $\partial F_I / \partial y_I$, towards a peak load F_I^m, which corresponded to the onset of the freeze bond failures. After F_I^m, with increasing y_I, the F_I decreased steeply. During this steep decrease, the freeze bonds failed through the rubble thickness on distinct zones around the indentor perimeter, that is, a global rubble failure occurred.

The virtual experiments were conducted on four different ridge geometries, which differed by the positions and locations of the rubble blocks (not by the keel thickness nor boundary conditions). The peak load F_I^m values depended on the rubble geometry. This difference was related to the initial failure patterns of the rubble, as illustrated by Fig. 4.11: In the case of a ridge yielding a higher load (Fig. 4.11a), a plug of rubble that becomes separated from the rest of the rubble is clearly larger than in the case of a ridge yielding a lower load (Fig. 4.11b). A relation between the buoyant load of the rubble plug forming in the initial failure and the peak load F_I^m was found, as shown in Publication IV. In other words, the dependency of F_I^m on ridge geometry was related to the difference in the buoyant load component due to the rubble plug (see Fig. 1.2) forming during the initial failure.

Furthermore, the F_I^m increased with freeze bond shear strength τ_{cr}, as

[2]The symbols from Publication IV have been changed here to match the notation used in earlier text. The following substitutions were made: $F \rightarrow F_I$ and $F^m \rightarrow F_I^m$.

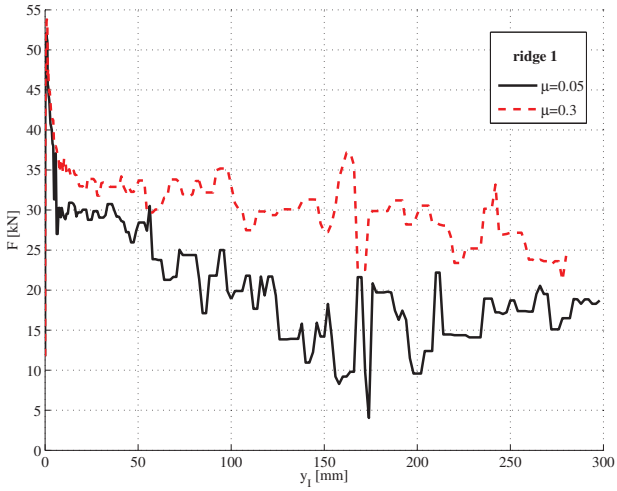

Figure 4.10. Indentor force-displacement ($F - y_I$) records from simulations of a punch through experiments on a partly consolidated ridge with two different friction coefficient μ values.

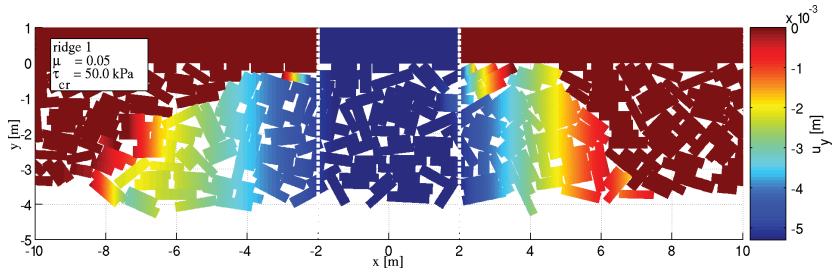

(a)

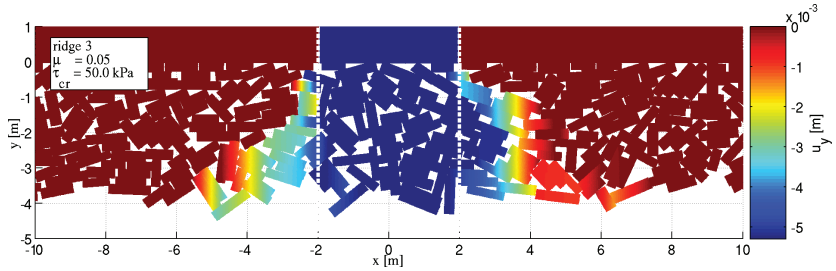

(b)

Figure 4.11. Rubble deformation patterns for two different ridge geometries after indentor penetration of $y_I = 5$ mm: ridge in (a) yielded ~ 50 % higher indentor load than ridge in (b). Colors indicate vertical displacement u_y of the rubble, with the displacing rubble mass being clearly larger in (a) than in (b). It can be noticed that the displacing rubble mass clearly reached an area wider than the indentor perimeter (indicated by thick white dashed lines).

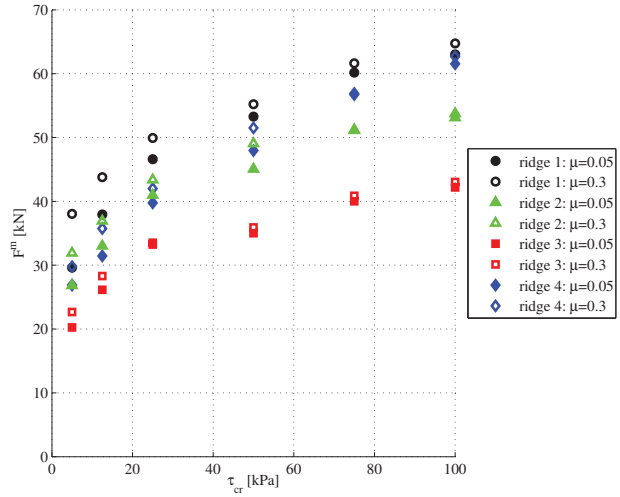

Figure 4.12. Maximum load F_I^m as a function of critical freeze bond shear strength τ_{cr}. The marker fill color in the figure indicates the F_I^m values from simulations with different friction coefficients μ, as shown by the legend.

shown in Fig. 4.12. As the figure shows, the rate $\partial F_I^m / \partial \tau_{cr}$ was not constant: The rate was higher with a low than with a high τ_{cr}. This feature could also be explained by the rubble deformation patterns. In the case of a weakly bonded rubble (here up to $\tau_{cr} = 50$ kPa), the amount of displacing rubble increased with the τ_{cr}, hence the increase in the F_I^m was driven by an increase in the buoyancy of the displacing rubble and the rubble cohesion. On the other hand, in the case of strongly bonded rubble ($\tau_{cr} \geq 50$ kPa), the deformation patterns remained approximately constant with change in τ_{cr}, and the increase in the F_I^m with τ_{cr} was only due to the change in rubble cohesion.

The rubble shear strength τ derived from the peak load F_I^m values were in the range of the full-scale experiment results. The derivation of τ from F_I^m was critically discussed. In the discussion, the estimates for the buoyant load component (such as F_I^r in Eq. 2.1) were considered. It was shown that the buoyant component of the displacing rubble must be carefully taken into account when deriving τ. As an example, the case of the simulations in Fig. 4.11 can be considered. From the figures, it can be seen that the area of the displacing rubble clearly extends beyond the perimeter of the indentor. If in this case the commonly used assumption that only the rubble plug directly under the indentor ($\alpha = 0°$ in Fig. 1.2) causing the buoyant load should be used, τ of the rubble becomes drastically overestimated.

The post-peak load, after the initial steep decrease in F following the peak load F_I^m, usually decreased in the simulations. This decrease in the load was due to the rubble plug, which formed during the initial failure and then dissolved as it moved downwards with the indentor. Hence, the physical phenomenon behind the load decrease was related to a change in the rubble geometry during an experiment. Usually, the decrease in the post-peak load levels has been accounted for the softening of the rubble material.

The effect of the block contact friction coefficient μ on the maximum load depended on the freeze bond strength: In the case of the weakest freeze bonds, an increase of μ from 0.05 to 0.3 increased the maximum load F_I^m by up to 28%, whereas with high freeze bond strengths the increase in F_I^m was negligible. This negligible effect was due to the bonds failing mainly under tension in the case of the strong freeze bonds. Since the block contact friction is related to the rubble internal friction angle, but does not affect the maximum load of a strongly bonded rubble, it was concluded that punch through experiments may not always be a suitable method for deriving friction angle for the rubble.

The simulation results were in fair agreement with earlier experimental data. As already mentioned above, the rubble shear strength values were in the range of full-scale punch through experiments. In addition, the deformation patterns were similar to those observed in the laboratory. The comparison to earlier modeling results showed some differences, for example, the tensile freeze bond failures are not predicted by the continuum models. These differences are likely the result of some phenomena being rendered out from the earlier results due to the continuum description of the rubble. This demonstrates a need to model the rubble using the discontinuous approach: Understanding the behavior of the ice rubble can be increased by small-scale results provided by discrete modeling of the rubble.

5. Conclusions and future work

In this thesis experimental and numerical studies on sea ice ridge keel punch through experiments were performed. The experiments were carried out to study laboratory-scale punch through experiments as a testing method. In the numerical modeling, emphasis was put on interpreting the punch through experiment results. The modeling methods used were based on a discontinuous description of the rubble material. The modeling methods were developed further for ice mechanics-related problems. The main original findings and features presented in this thesis are as follows:

1. The effect of the loading rate in the laboratory-scale punch through experiments was investigated, and it was found to be at least partly related to the experimental set-up instead of to the material properties of the rubble (Publication II).

2. Slow laboratory-scale punch through experiments were successfully modeled using the 3D discrete element method. The experiments with low indentor velocities were analyzed using the model (Publication III).

3. A clear relation between the rubble deformation patterns and force displacement records of the punch through experiments on non-cohesive rubble was found and analysed (Publications I and III).

4. A numerical model for a partly consolidated ice rubble based on discrete numerical modeling and initially rigid cohesive elements was developed and implemented (Publication IV).

5. The contact friction of the rubble blocks was found to affect the maxi-

mum indentor load values in the case of non-cohesive and weakly bonded rubble (Publications I and IV), but not in the case of strongly bonded rubble (Publication IV).

6. The initial failure pattern of partly consolidated rubble was shown to be related to the maximum load values in the punch through experiments. It was shown that if this relation is not taken into account, the material properties of the rubble may be incorrectly assessed (Publication IV).

7. The post-peak decrease in indentor load in punch through experiments is likely due to changes in the rubble geometry rather than to rubble material softening (Publication IV).

Since, by their very nature, ice ridges come in a variety of shapes and block sizes, future work on modeling should include more detailed investigations on the reasons behind the effect of the ridge geometry in the case of partly consolidated rubble. The work on the issue should involve various rubble depths, block geometries, and indentor widths so that the potential scale effects could be included into the analysis. Respectively, the packing, inner structure, and the detailed morphology of the natural ice ridges should be studied in order to fully ensure the resemblance between the modelled and natural ridges. In addition, the model should be used in parallel for virtual punch through and shear box experiments on ice rubble. This type of modeling should increase understanding on material modeling of ice rubble.

Furthermore, the model should be used in parallel with readily existing and potential new models based on the continuum description of the rubble. This is necessary, because large-scale problems may still be more efficiently solved using the continuum models, and most of the commercial codes used are based on the finite element method. On the other hand, the development of the continuum models can benefit from an understanding on the smaller scale phenomena provided by the discrete models. In other words, the advantage of the complementary roles of the discontinuum and continuum modeling should be exploited for the efficient and realistic modeling of ice mechanics problems.

Since the rubble failure process in the simulations of partly consolidated rubble involved tensile freeze bond failures, experimental work on freeze bond strength should be performed under various relative stresses, in-

cluding experiments under tensile stresses. Related to the experimental work, future work on the modeling of the punch through experiments should also include detailed identification of the relations between the quantities measurable in the field experiments and the material parameters of the rubble. This work would make it easier to interpret the results of the experiments, even when only a limited set of measurements in full-scale (in often very challenging environment) can be conducted.

Bibliography

Azarnejad, A. and Brown, T. (2001). Small-scale plane strain punch tests. *Journal of Cold Regions Engineering*, 15(3):135–153.

Azarnejad, A., Frederking, R., and Brown, T. (1999). Ice rubble strength from small scale punch through tests. In *Proceedings of OMAE99, 19th International Conference On Offshore Mechanics and Artcic Engineering*, pages 1–9.

Block, G., Rubin, M., Morris, J., and Berryman, J. G. (2007). Simulations of dynamic crack propagation in brittle materials using nodal cohesive forces and continuum damage mechanics in the distinct element code LDEC. *International Journal of Fracture*, 144(3):131–147.

Bruneau, S., Crocker, G., McKenna, R., Croasdale, K., Metge, M., Ritch, R., and Weaver, J. (1998). Development of techniques for measuring in situ ice rubble shear strength. In *Ice in Surface Waters, Proc. of the 14th International Symposium on Ice, IAHR*, volume 2, pages 1001–1007, Potsdam, New York, USA.

Camacho, G. and Ortiz, M. (1996). Computational modelling of impact damage in brittle materials. *International Journal of Solids and Structures*, 33(20–22):2899–2938.

Croasdale, K. R., Bruneau, S., Christian, D., Crocker, G., English, J., Metge, M., and Ritch, R. (2001). In-situ measurements of the strength of first-year ice ridge keels. In *Proceedings of the 16th International Conference on Port and Ocean Engineering under Arctic Conditions, POAC'01*, volume 3, pages 1445–1454, Ottawa, Ontario, Canada.

Cundall, P. and Strack, O. (1979). A discrete numerical model for granular assemblies. 29:47–65.

Ettema, R. and Schaefer, J. A. (1986). Experiments on freeze-bonding between ice blocks in floating ice rubble. *Journal of Glaciology*, 32(112):397–403.

Ettema, R. and Urroz, G. E. (1989). On internal friction and cohesion in unconsolidated ice rubble. *Cold Regions Science and Technology*, 16(3):237–247.

Haase, A., Polojärvi, A., and Tuhkuri, J. (2010). 3D discrete numerical modelling of conical structure-ice rubble interaction. In *Proceedings of 20th IAHR International Symposium on Ice, IAHR, Lahti, Finland (electronic publication).*

Heinonen, J. (2004). *Constitutive modeling of ice rubble in first-year ridge keel*. Doctoral Thesis, TKK. VTT Publications 536. Espoo, Finland, 2004, 142 p, ISSN 1235-0621.

Heinonen, J. and Määttänen, M. (2000). Ridge loading experiments, field experiments in winter 2000. LOLEIF Progress Report No. 10, TKK. 40 p.

Heinonen, J. and Määttänen, M. (2001a). Full-scale testing of ridge keel mechanical properties in loleif project. In *Proceedings of the 16th International Conference on Port and Ocean Engineering under Arctic Conditions, POAC'01*, volume 3, pages 1435–1444, Ottawa, Ontario, Canada.

Heinonen, J. and Määttänen, M. (2001b). Ridge keel mechanical properties - Testing. Field experiments in winter 2001. ReportSTRICE, TKK. 39 p.

Heinonen, J. and Määttänen, M. (2001c). Ridge keel mechanical properties - testing. field experiments in winter 2001. -reportSTRICE, TKK. 39 p.

Hopkins, M. (1992). Numerical simulation of systems of multitudinous polygonal blocks. Technical Report 92-22, Cold Regions Research and Engineering Laboratory, CRREL. 69 p.

Hopkins, M. (1998). Four stages of pressure ridging. *Journal of Geophysical Research*, 103(C10):21,883–21,891.

Hopkins, M., Tuhkuri, J., and Lensu, M. (1999). Rafting and ridging of thin ice sheets. *Journal of Geophysical Research*, 104(C6):13605–13613.

Jensen, A., Løset, S., Høyland, K. V., Liferov, P., Heinonen, J., Evers, K.-U., and Määttänen, M. (2001). Physical modelling of first-year ice ridges - part II: Mechanical properties. In *Proceedings of the 16th International Conference on Port and Ocean Engineering under Arctic Conditions, POAC'01*, volume 3, pages 1493–1502, Ottawa, Ontario, Canada.

Kuroiwa, D. (1961). A study of ice sintering. *Tellus*, 13(2):252–259.

Lemee, E. and Brown, T. (2002). Small-scale plane strain punch tests. In *Ice in the Environment: Proceedings of the 16th IAHR International Symposium on Ice, Dunedin, New Zealand.*, volume 2, pages 1–7.

Leppäranta, M. and Hakala, R. (1989). Field measurements of the structure and strength of first-year ice ridges in the baltic sea. In *Eighth International Conference on Offshore Mechanics adn Arctic Engineering, Hague, Netherlands*, volume 4, pages 169–174.

Leppäranta, M. and Hakala, R. (1992). The structure and strength of first-year ice ridges in the baltic sea. *Cold Regions Science and Technology*, 20(3):295–311.

Liferov, P. and Bonnemaire, B. (2005). Ice rubble behaviour and strength: Part I. review of testing and interpretation of results. *Cold Regions Science and Technology*, 41:135–151.

Liferov, P., Jensen, A., and Høyland, K. (2002). On analysis of punch tests on ice rubble. In *Proceedings of the 16th International Symposium on Ice*, volume 2, pages 101–110, Dunedin, New Zealand.

Liferov, P., Jensen, A., and Høyland, K. (2003). 3D finite element analysis of laboratory punch tests on ice rubble. In *Proceedings of the 17th International Conference on Port and Ocean Engineering under Arctic Conditions, POAC'03*, volume 2, pages 611–621, Trondheim, Norway.

Morris, J. P., Rubin, M., Block, G., and Bonner, M. (2006). Simulations of fracture and fragmentation of geologic materials using combined FEM/DEM analysis. *International Journal of Impact Engineering*, 33(1-12):463–473.

Munjiza, A. (2004). *The combined finite-discrete element method*. John Wiley & Sons Ltd., Chichester, England.

Munjiza, A. and Andrews, K. (1998). Contact detection algorithm for bodies of similar sizeNBS. *International Journal for Numerical Methods in Engineering*, 43(1):131–149.

Munjiza, A. and Andrews, K. (2000). Penalty function method for combined finite-discrete element systems comprising large number of separate bodies. 49(11):1377–1396.

Munjiza, A., Owen, D., and Bićanić, N. (1995). A combined finite-discrete element method in transient dynamics of fracturing solids. 12:145–174.

Ortiz, M. and Pandolfi, A. (1999). Finite-deformation irreversible cohesive elements for three-dimensional crack propagation analysis. *International Journal for Numerical Methods in Engineering*, 44:44–1267.

Paavilainen, J. and Tuhkuri, J. (2012). Parameter effects on simulated ice rubbling forces on a wide sloping structure. *Cold Regions Science and Technology*, (doi:10.1016/j.coldregions.2012.04.005).

Paavilainen, J., Tuhkuri, J., and Polojärvi, A. (2006). Discrete element simulation of ice pile-up against an inclined structure. In *Proceedings of the 18th International Symposium on Ice, IAHR*, volume 2, pages 177–184, Sapporo, Japan.

Paavilainen, J., Tuhkuri, J., and Polojärvi, A. (2009). 2D combined finite–discrete element method to model multi-fracture of beam structures. *Engineering Computations*, 26(6):578–598.

Paavilainen, J., Tuhkuri, J., and Polojärvi, A. (2011). 2D numerical simulations of ice rubble formation process against an inclined structure. *Cold Regions Science and Technology*, 68(1-2):20–34.

Papoulia, K. D. and Vavasis, S. A. (2003). Time continuity in cohesive finite element modeling. *International Journal for Numerical Methods in Engineering*, 58:701.

Sam, C.-H., Papoulia, K. D., and Vavasisc, S. A. (2005). Obtaining initially rigid cohesive finite element models that are temporally convergent. *Engineering Fracture Mechanics*, 72(14):2247–2267.

Sayed, M., Timco, G. W., and Sun, L. (1992). Testing model ice rubble under proportional strains. In *OMAE 1992, Proceedings of the 11th International Conference On Offshore Mechanics and Artcic Engineering*, volume IV - Arctic/Polar Technology.

Serré, N. (2011). Mechanical properties of model ice ridge keels. *Cold Regions Science and Technology*, 67(3):89–106.

Tuhkuri, J. and Polojärvi, A. (2005). Effect of particle shape in 2D ridge keel deformation simulations. In *Proceedings of the 18th International Conference on Port and Ocean Engineering under Arctic Conditions, POAC'05*, volume 2, pages 939–948, Potsdam, New York, USA.

Aalto-DD 50/2013

ISBN 978-952-60-5081-2
ISBN 978-952-60-5082-9 (pdf)
ISSN-L 1799-4934
ISSN 1799-4934
ISSN 1799-4942 (pdf)

Aalto University
School of Engineering
Department of Applied Mechanics
www.aalto.fi

BUSINESS + ECONOMY

ART + DESIGN + ARCHITECTURE

SCIENCE + TECHNOLOGY

CROSSOVER

DOCTORAL DISSERTATIONS